Cyclic behavior of replaceable steel coupling beams

Xiaodong Ji[1], Yandong Wang[2], Qifeng Ma[3], Taichiro Okazaki [4]

[1]*Associate professor, Key Laboratory of Civil Engineering Safety and Durability of China Education Ministry, Department of Civil Engineering, Tsinghua University, Beijing 100084, China*

[2]*Graduate student, Beijing Engineering Research Center of Steel and Concrete Composite Structures, Department of Civil Engineering, Tsinghua University, Beijing 100084, China*

[3]*Graduate student, Department of Civil Engineering, Tsinghua University, Beijing 100084, China*

[4]*Associate professor, Graduate School of Engineering, Hokkaido University, Sapporo, Hokkaido 060-8628, Japan*

Abstract: For improving the seismic resiliency of coupled shear wall systems, a type of replaceable steel coupling beam is developed, which consists of a central "fuse" shear link, connecting to steel beam segments at its two ends. Inelastic deformation is concentrated in the shear link during a severe earthquake, and the damaged links can be replaced easily as specialized link-to-beam connections are adopted. This paper presents a series of quasi-static tests conducted to examine the seismic behavior and replaceability of the replaceable coupling beams. A total of four large-scale specimens were designed and tested, where different types of beam-to-link connections were adopted, including the end plate connection, splice plate connection, bolted web connection and adhesive web connection. All specimens fully developed the shear strength of "fuse" links and showed large inelastic rotation capacity

Please cite this article as: Xiaodong Ji, Yandong Wang, Qifeng Ma, Taichiro Okazaki. Cyclic behavior of replaceable steel coupling beams. Journal of Structural Engineering, 2017, 143(2): 04016169.
doi: 10.1061/(ASCE)ST.1943-541X.0001661

of no less than 0.06 rad, except for the specimen with adhesive web connection that failed at an early stage. The specimen with end plate connection had inelastic deformation concentrated in the shear link, showing very stable hysteresis behavior. Slippage of high-strength bolts was observed at the splice plate connection and bolted web connection, which led to increased deformation and “pinching” in hysteresis loops of coupling beams. Interestingly, at coupling beam rotation exceeding 0.01 rad, large axial force developed in the steel coupling beams, the maximum value of which reached approximately a quarter to half of the axial yield strength of the shear link. In addition, on-site replacement of shear links was demonstrated after the coupling beam specimens experienced 0.02 rad rotation. The end plate connection was replaced within the shortest time, while the bolted web connection was able to accommodate the largest residual deformation.

Keywords: replaceable steel coupling beam; shear link; link-to-beam connection; cyclic behavior; replaceability; axial force

Introduction

Recent large earthquakes, including the 2008 China earthquake, 2010 Chile earthquake, 2011 Japan earthquake and 2011 New Zealand earthquake, have demonstrated that modern buildings generally behave well in terms of life safety. However, post-damage repair of these buildings was found to be costly in both expense and time, leading to long-lasting loss of occupancy and slow recovery of community. For minimum disruption in life and business of the urban society, prompt recovery of buildings is a clear need. One solution to achieve this is to use easily replaceable components or devices in energy dissipation regions (i.e., plastic hinges) of the structure.

Coupled wall systems are often used in high-rise buildings due to the superior strength and stiffness they provide. In such a system, coupling beams distributed along the building height are designed as the components that undergo inelastic deformation and dissipate seismic energy. However, traditional reinforced concrete (RC) coupling beams are prone to non-ductile failure, and post-damage repair of them is expensive and time-consuming. Recently, various types of replaceable coupling beams have been proposed and recognized as an alternative to traditional RC coupling beams (e.g., Fortney et al. 2007; Chung et al. 2009; Kumagai et al. 2009, Christopoulos and Montgomery 2013; and Lu et al. 2013).

Fig. 1 shows a type of replaceable steel coupling beam, which comprises a central “fuse” shear link connected to steel beam segments at its two ends. By appropriately proportioning the beam segments and shear link, the inelastic deformation and damage can concentrate in the “fuse” shear links during a severe earthquake. Extensive studies (e.g., Malley and Popov 1984, Kasai and Popov 1986; Popov and Engelhardt 1988; Okazaki et al. 2005; Okazaki and Engelhardt 2007; Ji et al. 2016) have indicated that a short shear link with proper detailing can provide very stable, ductile and predictable behavior under cyclic shear loading. On the other hand, the success of the proposed replaceable steel coupling beams relies on the specialized connections between the link and normal beam segments (referred to as "link-to-beam connection" hereinafter) that allow the damaged link to be replaced in the presence of residual drifts expected after a severe earthquake event.

This paper presents four types of specialized link-to-beam connections, i.e., the end plate connection, splice plate connection, bolted web connection and adhesive web connection. Large-scale specimens of replaceable coupling beams that adopted these four types of link-to-beam connections were tested to examine their cyclic behavior and replaceability. The testing concept in this paper is similar to McDaniel et al. (2003) and Mansour et al. (2011) which target to develop replaceable "fuse" links used in bridge towers and used in eccentrically braced frames (EBFs), respectively. The first section presents the specimen design and experimental program. In the second section, the test results are detailed, including hysteretic behavior, failure modes, strength and inelastic rotation capacity, and the axial force developed in the coupling beam. The third section compares the behavior of various link-to-beam connections and describes its influence on deformation and energy dissipation capacities of coupling beams. Finally, the on-site replaceability of shear link is examined and discussed.

Experimental program

Test specimens

The test specimens are representative of the coupling beams at the fifth floor of an eleven-story, 48.4 m tall building. As shown in Fig. 2, the building has a plan dimension of 48.6 m by 14.4 m. The building adopts a RC shear wall-frame system. The structure was designed according to the Chinese code for seismic design of buildings [GB 50011-2010 (CMC 2010)]. The seismic load was considered for a high seismic area in Beijing, where the peak ground acceleration of the design basis earthquake (DBE, with a probability of exceedance of 10% in 50 years) equals 0.2 g. The structure had a fundamental period of 1.35

s in the transverse direction. Nonlinear analysis of the structure was conducted using OpenSees software, where shear walls were modelled by multi-layer shell element (Ji et al. 2015a) and replaceable coupling beams by nonlinear link element. Seven records of motions were selected and scaled as the input motions. Nonlinear dynamic analysis indicates that the maximum story drift of the structure is 0.8% when subjected to the maximum considered earthquake (MCE, with a probability of exceedance of 2% in 50 years) motions, and the corresponding rotation of the replaceable coupling beams is less than 0.02 rad. The residual rotation of coupling beams after MCE motions is merely 0.002 rad. It is noted that the Chinese code for seismic design of buildings [GB 50011-2010 (CMC 2010)] requires stricter drift limits for building structures than ASCE 7-10 code (ASCE 2010) for earthquake loads.

The specimens were fabricated at 5/6 scale of the prototype coupling beam. A total of four specimens were designed, each used different type of link-to-beam connections (Ji et al., 2015b). Fig. 3 shows the geometry and details of the specimens. End plate connection was used for Specimen CB1, splice plate connection for CB2, bolted web connection for CB3 and adhesive web connection for CB4. Design for these connections will be detailed later.

Shear link

Table 1 summarizes the design parameters of shear links for all specimens. All shear links were built-up sections. The links of Specimens CB1 and CB2 were I-shaped sections, while those of Specimens CB3 and CB4 were back-to-back double channel sections. The flanges and web were welded by complete-joint-penetration (CJP) groove welds. Both the link flange and web satisfied the requirement for highly ductile members by the AISC 341-10 provisions

(AISC 2010). All links had a length ratio, $e/(M_p/V_p)$, smaller than 1.6 and, therefore, they were expected to yield primarily in shear. Note that e denotes the link length (see Fig. 3), and M_p and V_p denote the plastic flexural strength and shear strength of the link, respectively, calculated based on the actual measured yield strength of the steel and actual measured dimensions. The prototype links were designed with short length to limit their weight for easy replacement. The maximum weight of the link specimens was 85 kg, which is 63% of the prototype link.

The stiffeners of shear link were full depth, welded to the link web and to both link flanges using fillet welds, and they were set on one side of the web only. The AISC 341-10 provisions (AISC 2010) require intermediate web stiffeners to be spaced at intervals not exceeding ($30t_w$-d/5), where t_w denotes the web thickness and d denotes the link depth. The stiffener spacing for shear links of Specimens CB1 and CB2 satisfied this limit, while that for Specimens CB3 and CB4 violated the limit by 35%. The reason for increasing the stiffener spacing of the latter two specimens is to suppress the negative influence of welding on those thin webs. To delay web fracture at the region where the flange-to-web CJP groove weld and the fillet welds of the stiffeners meet, the vertical fillet welds of the web stiffeners were terminated at a distance of no less than five times the web thickness from the flange-to-web weld (McDaniel et al. 2003; Okazaki et al. 2005).

All links of the specimens adopted hybrid sections. The link flanges were made of Q345 steel (nominal yield strength f_y = 345 MPa), and the stiffeners of Q235 steel (f_y = 235 MPa). The link webs for Specimen CB1 and CB2 were made of low-yield-strength steel LY225 (f_y =

225 MPa), and those for Specimen CB3 and CB4 were made of Q235 steel. Table 2 lists the material properties for steel of shear links measured by tensile coupon tests.

Beam segment

The beam segments of all specimens were built-up I-shaped steel, as shown in Fig. 3. All beam segments were made of Q345 steel. To ensure that the beam segments remain elastic when the shear link fully yielded and strain-hardened, their strength was designed to exceed the strength demand corresponding to the overstrength of shear link. The overstrength factor of shear links of Specimens CB3 and CB4 was taken as 1.5 per the AISC 341-10 provisions (AISC 2010a). Shear links of Specimens CB1 and CB2 had a very small length ratio of 0.7 and their overstrength factor was taken as 2.0 as suggested by Ji et al. (2016).

Link-to-beam connections

The link-to-beam connections shall be provided a strength that exceeds the overstrength capacity of the shear link, and shall enable replacement of damaged shear links. The four types of link-to-beam connections examined in this program are described in the following.

(1) End plate connection (see Fig. 3(a))

The shear link was connected to the extended end plate using CJP welds. The link end plate was spliced to the end plate of the beam segment. Horizontal stiffeners were added on the beam segments at the flange height of the shear link. The end plates of the shear link were fabricated with a shear key and that of beam segment with a corresponding groove. The shear link was installed horizontally allowing the shear key to slide along the groove, and then the end plates were clamped using high-strength bolts. The difference between this end plate connection and that described in Mansour et al. (2011) is the presence of shear key that can significantly increase the shear strength of the connection.

As shown in Fig. 4(a), the connection was designed such that the shear key transfers the shear force and the high-strength bolts resist the bending moment. The end plate thickness and high-strength bolt diameter were determined following a design procedure for end plate connections specified by the AISC Design Guide Series 4 (Murray and Summer, 2003). As the end plate of shear link might yield under large tensile force of flanges, the prying action and its resulting additional force in high-strength bolts was considered in design. Note that, without the shear key, the maximum number of high-strength bolts that the connection space allows for cannot meet the strength demand of the connection subjected to combined shear force and bending moment. The replaceablity of the connection will be discussed later.

(2) Splice plate connection (see Fig. 3(b)).

The link web was spliced to the beam web in double shear, similar as that described in Fortney et al. (2007). Horizontal stiffeners were welded on the beam segments at the flange height of the shear link. The link flanges were spliced to the horizontal stiffeners of the beam segments in double shear. High-strength bolts were used for the connection. As shown in Fig. 4(b), the flange splices were designed to resist all the moment at the centerline of the splice, and the web splices were designed to resist all the shear force acting at the centerline of the splice as recommended by Kulak and Green (1990). The number and size of bolts in the web slice plate were determined based on the eccentric shear strength, which is calculated by the method of instantaneous center of rotation with the bolt load-deformation relationship developed by Kulak et al. (1987).

(3) Bolted web connection (see Fig. 3(c)).

The shear link consisted of back-to-back double channel sections, sandwiching the web of the beam segment through an eccentrically loaded bolted connection. This bolted web connection was identical to that described in Mansour et al. (2011), and was designed following the procedure they proposed. As shown in Fig. 4(c), the eccentric shear strength of the connection was estimated using the method of instantaneous center of rotation and with the bolt load-deformation relationship developed by Kulak et al. (1987). The strength demand of the connection was taken as a shear force of ΩV_{pn} applied with an eccentricity equal to the distance between the instantaneous center of connection rotation and the link mid-span. To prevent the connection failure due to excessive bolt-hole ovalization of the thin web, the link webs in the connection region were reinforced by 6-mm thick plates.

(4) Adhesive web connection (see Fig. 3(d))

A double channel link was connected with the web of the beam segment through web connection, similarly to the bolted web connection, but by use of epoxy adhesive instead of high-strength bolts. Four erection bolts were placed to keep the link in place while the adhesive cured. Note that the adhesive can develop its nominal strength within 24 hours at normal temperature. These erection bolts were tightened to ensure that the connected pieces remain in contact, but not fully pretensioned so as not to squeeze the adhesive out. As failure of adhesive is brittle, the eccentric shear strength provided by adhesive was assessed by elastic analysis, which is similar to the traditional elastic (vector) analysis for the strength of bolt group (Salmon et al. 2009). In this analysis, the connection area is considered as an elastic cross-section subjected to combined torsion moment and direct shear, as shown in Fig. 4(d). The connection arrives at its maximum strength when the critical point reaches the shear stress capacity of epoxy adhesive, which was taken as its nominal shear strength of 15 MPa. The eccentric shear strength provided by the bolts in bearing was calculated using the elastic (vector) analysis as well. The total strength of the eccentric shear connection was calculated as the sum of the strengths provided by these two parts. This simple superposition might result in an overestimation of the connection strength as the adhesive and bolts may develop their strength at different stage of deformation, which will be discussed later. The replacement of shear link might be achieved by heating the adhesive until it loses strength.

All high-strength bolts used in the specimens had a strength grade of 10.9 (minimum tensile strength f_u = 1000 MPa, and strength ratio f_y/f_u = 0.9). M30 bolts were used for Specimens CB1, CB3 and CB4, and M24 bolts for Specimen CB2. All bolt holes had standard size per the AISC 360-10 provisions (AISC 2010b). For Specimens CB1 through CB3, high-strength bolts were installed by a calibrated wrench to obtain their specified pretension forces. Steel surfaces of connected pieces were unpainted blast-cleaned, and the slip coefficient was assumed as 0.45 per Chinese code for design of steel structures [GB 50017-2003 (CMC 2003)].

Test setup, instrumentation and loading protocol

Fig. 5 shows the test setup. The coupling beam specimen was securely clamped to two steel frame columns. These frame columns were designed with large stiffness to simulate the constraint of adjacent wall piers to coupling beam. The columns were pinned to the foundation beam at one end and pinned to the rigid loading beam at the other end. Note that, as required by the AISC 341-10 (AISC 2010), the steel coupling beam must be adequately embedded with the RC wall piers such that its full capacity can be developed. Past tests (e.g., Shahrooz et al. 1993) indicate that the embedded beam-wall connection is not fully rigid, and its local behavior may lead to additional rotation at the end of coupling beams. The test setup of this program does not include this local deformation in beam-wall connection, as the bolted end-plate connection to the loading frame column is relatively rigid.

Instrumentation was used to measure the load, displacements and strains of the specimen, as shown in Fig. 5. Shear force of the coupling beam was calculated from the lateral load measured by load cell. Chord rotation of the coupling beam (referred as to “beam rotation” hereinafter), with the length taken as the face-to-face distance between the beam end plates, was measured by crossed linear variable differential transformers (LVDTs) D1 and D2. Rotation of the shear link (referred as to “link rotation”) was measured by crossed LVDTs D3 and D4. Strain gauges measured the strains of both shear link and beam segments.

Fig. 6 shows the loading protocol of the test. The loading included two phases. In Phase I, the specimen was loaded up to 0.02 rad rotation, approximately the rotation demand of the prototype coupling beam under MCE. Afterwards, the shear link was replaced with a new link. In Phase II, the specimen with replacement shear link was loaded till complete failure. For each phase, cyclic loading was force-controlled before the shear link yielded, and two levels of shear forces (i.e., $0.5V_p$ and V_p) were considered. After yielding of link, the loading was changed to displacement control. The rotation of coupling beam increased in increments of 0.005 rad before 0.02 rad beam rotation and then increased in increments of 0.01 rad. Two cycles were repeated at each level of loading.

Experimental result

Hysteretic response

Phase I loading

Fig. 7 shows the hysteretic responses of shear force versus coupling beam rotation for all specimens in the Phase I loading. Specimens CB1 and CB2 showed very stable hysteretic behavior. Slight slippage of high-strength bolts in the web connection was observed for Specimen CB3, resulting in a slight "pinching" of hysteresis loops. Non-ductile failure occurred when Specimen CB4 arrived at 0.005 rad rotation, which is induced by the brittle failure of adhesive in the link-to-beam connection. The reason for the connection failure will be discussed later.

The links of these specimens yielded in shear and developed overstrength. Two values of plastic strength of shear link are indicated in each figure. The nominal value of plastic strength V_{pn} was calculated using the nominal yield strength of the steel and nominal dimensions, while the measured value V_p was based on the measured yield strength of the steel and measured dimensions. These two values were nearly identical for the links of Specimens CB1 and CB2 because the measured yield strength for LY225 steel was nearly identical to the nominal strength. However, the value of V_p was 34.5% higher than V_{pn} for the links of Specimen CB3 and CB4 due to the difference between nominal and measured yield strength of Q235 steel.

Phase II loading

Fig. 8 shows the hysteretic responses of Specimens CB1 through CB3 in the Phase II loading. Specimen CB4 was not considered in the Phase II loading because of early-stage failure of the adhesive web connection. Specimen CB1 showed stable hysteretic loops even under very large inelastic rotation. Specimens CB2 and CB3 exhibited different levels of "pinching" in hysteretic loops due to slippage of high-strength bolts. After the bolts bore against the bolt holes or the web splice plates bore against the link and beam flanges, the shear force increased again.

Fig. 8 also shows the hysteretic responses of shear links in the Phase II loading. The shear links of Specimens CB1 and CB2 showed full and symmetrical hysteretic loops, with large inelastic rotation and stable energy dissipation. However, the hysteretic loop of the shear link of Specimen CB3 was unsymmetrical, with a maximum rotation of 0.04 rad in positive loading and 0.12 rad in negative loading. This is because, due to the intentional residual rotation, the bolts could not be centered in the bolt holes when the replacement shear link was installed. The bolts slipped for a larger distance in the positive loading, which increased the connection rotation and accordingly decreased the link rotation. It is notable that all links developed a high level of overstrength after yielding in shear.

Failure mode

Strain measurement indicates that beam segments remained elastic for the duration of the test. All damage occurred in shear links and connections. Table 3 summarizes the process of visually identified damage and the cause of ultimate failure. In this paper, failure of the specimen is defined as the point where the shear strength drops to below the link plastic strength V_p. Note that the values in this table corresponded to the damage for Specimens CB1 through CB3 in the Phase II loading, while the damage for Specimen CB4 in the Phase I loading.

Bolt slippage was clearly observed at 0.03 rad coupling beam rotation for Specimens CB2 and CB3, and slippage of the connection of Specimen CB3 was more severe than that of Specimen CB2. High-strength bolts of Specimen CB1 did not slip because the shear keys prevented relative translation between the end plates. Web buckling, stiffener-to-flange weld fracture, web fracture and flange-to-end plate weld fracture were observed in shear links, which are consistent with past test observations (McDaniel et al. 2003; Okazaki et al. 2005; Ji et al. 2016). The shear link of Specimen CB3, which violated the stiffener spacing limit, showed more severe web buckling than other specimens.

Fig. 9 shows photographs of the specimens and a close look at the primary failure mode. Specimen CB1 failed by fracture of the link flange-to-end plate weld (see Fig. 9(b)), which was likely caused by low-cycle fatigue of tensile and compressive strains coupled with local bending of the link flange. Specimens CB2 and CB3 failed by link web fracture (see Fig. 9(d) and (f)), which initiated at the termination of a fillet weld connecting a stiffener to the web and then propagated along the stiffener-to-web weld. Specimen CB4 failed by the adhesive fracture in beam-to-link connection (see Fig. 9(h)).

Shear strength

Table 4 presents the values of link plastic shear strength V_p and maximum shear strength V_{max} of the specimens. For Specimens CB1 through CB3, V_{max} is governed by the maximum strength of shear link and, therefore, the value of $\Omega = V_{max}/V_p$ represents the overstrength of the shear links. The overstrength of the I-shaped links of Specimens CB1 and CB2 that had a length ratio of 0.7 was approximately 2.0, significantly exceeding the value of 1.5 specified for EBF links in AISC 341-10 (AISC 2010). These values of overstrength for very short links are consistent with past findings by Ji et al. (2016). The overstrength of the double channel link of Specimen CB3 that had a length ratio of 1.24 was equal to 1.57. The shear link of Specimen CB4 did not fully develop its strength because of the failure of adhesive web connection.

Inelastic rotation capacity

Table 5 lists the inelastic rotation capacity of the coupling beam specimens, which is taken as the maximum rotation sustained for at least one full cycle of loading prior to failure. Specimens CB1 through CB3 developed an inelastic rotation of no less than 0.06 rad.

Table 5 also summarizes the inelastic rotation capacity and cumulative plastic rotation of shear links. The very short I-shaped shear links used in Specimens CB1 and CB2 had an inelastic rotation of over 0.14 rad, significantly larger than 0.08 rad assumed for shear links in the AISC 341-10 provisions (AISC 2010). These shear links achieved a cumulative plastic rotation of over 4.0 rad. These values are consistent with the past test results for very short shear links with LYP 225 steel web (Ji et al. 2016). The double channel link of Specimen

CB3 had an inelastic rotation of 0.12 rad and cumulative plastic rotation of 1.85 rad. It is notable that, although the double channel link had lower inelastic rotation than the I-shaped links, Specimen CB3 still developed a coupling beam rotation identical to that of CB1 owing to the additional deformation provided by bolted web connection.

Axial force in coupling beam

Axial deformation of shear links was observed in past tests where the shear links had no axial restraint during cyclic shear loading (Ji et al. 2016). In an actual coupled wall, however, the shear link is restrained by the adjacent wall piers and axial force is expected to develop at large rotations. In this test, the frame columns that connected with the coupling beam at its two ends were designed with sufficient stiffness to simulate the restraint induced by wall piers.

As shown in Fig. 5, five strain gauges were mounted on beam segment sections A and B of Specimen CB1. The curvature and average axial strain at a section was estimated by linear fitting of the measured strains over the depth to determine the strain distribution. As those beam sections remained elastic during testing, the moment and axial force at the section were calculated from the measured curvature and average axial strain by using the actual sectional geometry and using an assumed Young's modulus of steel of 2.05×10^5 N/mm^2 (see Fig. 5). The shear force in the coupling beam can be estimated from the bending moments at sections A and B. Fig. 10 (a) compares the shear force of Specimen CB1 calculated from the strain data with that obtained from load cell measurement. Good correlation between these two sets of data validates the reliability of the forces calculated from strain data. Fig. 10 (b) shows the curves of axial forces versus beam rotation of Specimen CB1. When the coupling beam was loaded to over 0.01 rad rotation, a large tensile force developed, followed by a large compressive force when the specimen unloaded to zero rotation. The maximum value of axial tensile force was 500 kN at 0.06 beam rotation, equal to a quarter of the yield axial strength of the shear link. The maximum value of axial compressive force was 800 kN, equal to approximately half of the yield axial strength of the shear link. Note that the magnitude of measured axial forces of Specimen CB2 was nearly identical to that of Specimen CB1. Because of failure of the strain gauges in Specimens CB3, no data on axial forces was obtained for Specimen CB3.

Comparing the results of this test program and past tests in Ji et al. (2016), the axial force was found to have a limited effect on the cyclic shear behavior of those short links that were designed following the AISC 341-10 provisions (AISC 2010a). The influence of axial forces on link-to-beam connections appears to be limited as well. However, large axial forces may affect the performance of the joints between coupling beams and wall piers, and cause redistribution of shear forces of the wall piers that are connected to the coupling beams (Teshigawara et al. 1998). The effect of axial forces shall be studied in future.

Connection behavior

Local deformation of end plate connection

The thickness of the link end plate of Specimen CB1 was 30 mm, less than the 35 mm required to fully prevent prying action estimated per the AISC Design Guide Series 4 (Murray and Summer, 2003). As shown in Fig. 11, the tensile link flange pulled the end plate and deflected it outward. The local plastic deformation of the end plate could contribute to rotation of the connection.

Bolt slippage in splice plate connection and bolted web connection

Substantial slip occurred repeatedly in Specimens CB2 and CB3. Fig. 12(a) shows a photograph of the beam segment web of Specimen CB2 after the web splice plate was removed post to the Phase II loading test. Wearing of the blast-cleaned surface near the bolt holes and ovalization of bolt-hole was observed. Fig. 12(b) shows slippage of high-strength bolts observed in the bolted web connection of Specimen CB3. Fig. 8(c) and (e) indicate decrease in slip resistance after repeated bolt slippage, which was likely because surface wear of the jointed pieces decreased the pretension forces in the high-strength bolts and the coefficient of friction.

Adhesive failure in adhesive web connection

For Specimen CB4, the adhesive peeled off from the corner of the web connection where the acting stress was expected to be maximum. As the shear failure of epoxy adhesive was very brittle, the fracture of adhesive expanded to the whole connection rapidly, leading to a sudden failure of the connection. Such brittle failure mode is unwanted for seismic design of replaceable coupling beam.

Overlap shear coupon tests were conducted to obtain the actual shear strength of the epoxy adhesive. Fig. 13 shows the details of the overlap coupon specimen where the steel plates were spliced in double shear through adhesive bonds. The average value of the shear strength of adhesive measured by three coupon test was 18 MPa, higher than its nominal strength of 15 MPa. However, the erection bolts did not develop their bearing strength at the small deformation when the adhesive failed. Note that, the measured maximum shear force of CB4 was very close to the eccentric shear strength of the adhesive calculated with the shear stress capacity of adhesive equal to 18 MPa. It is likely reasonable to neglect the contribution of the erection bolts in the calculation of the eccentric shear strength of the adhesive web connection.

Contribution on coupling beam rotation

Local deformation of end plates caused rotation of the end plate connection, and bolt slippage induced rotation of the splice plate connection and bolted web connection. These connection rotations provided additional deformation for coupling beams. Fig. 14 shows the ratio of the deformation induced by connection rotation Δ_{conn} over the total deformation of the coupling beam Δ_{beam}, where Δ_{conn} was calculated from the measured Δ_{beam} minus the measured link deformation and the elastic deformation of beam segments calculated from their bending moments and shear forces. At 0.02 rad coupling beam rotation, the ratio $\Delta_{\mathrm{conn}}/\Delta_{\mathrm{beam}}$ was 18% for Specimen CB1, 22% for CB2 and 40% for CB3. At 0.06 rad coupling beam rotation, the ratio remained 16% for Specimen CB1, while it increased to 40% for CB2 and 50% for CB3 due to increased slippage of high-strength bolts. Note that the plots in Fig. 14 were calculated based on the averaged deformation measured in both positive and negative loadings.

Effect on energy dissipation

Fig. 15 shows the cumulative energy dissipated by the specimens up to completion of the first cycle of 0.06 rad beam rotation. Since bolt slippage resulted in pinching in hysteresis loops of

Specimens CB2 and CB3, their cumulative energy dissipation was approximately 17% lower than that of Specimen CB1. For Specimens CB1, over 90% of the energy was dissipated by the shear link. For CB2, 80% of the energy was dissipated by the shear link and the other 20% was dissipated by the connections. For CB3, however, 41% of the energy was dissipated by the connection, as severe bolt slippage occurred in the bolted web connection.

Replaceability

Replacement of shear link was conducted by two technicians after the Phase I loading. First, the shear link was removed when the shear force was unloaded to zero. Then, the drift of loading frame was gradually decreased to find the maximum residual rotation φ_{re} that allows for easy reinstallation of new shear link without additional fabrication such as welding or postdrilling bolt holes. Afterwards, the new shear link was installed at the residual rotation of φ_{re}.

Specimen CB1 only took 0.4 h for replacement, while Specimens CB2 and CB3 took 2.6 and 2.2 h for replacement owing to the larger number of high-strength bolts. The residual rotation φ_{re} allowable for easy replacement was 0.0045 rad for Specimens CB1 and CB2, and 0.0065 rad for Specimen CB3. These values were larger than 0.002 rad, i.e., the estimated residual rotation of the coupling beams for the prototype structure subjected to MCE motions.

Setting gaps or distances is necessary for ensuring that new shear link can be installed. In this test, new shear links of Specimens CB1 and CB2 were 3 mm shorter than the clearance between the beam segments. A clearance of 2 mm was set between the shear key of new shear link of Specimen CB1 and the corresponding groove. Shim plates were used to fill the gaps between the plates and the clearance, and no adverse consequences in connection behavior were observed.

If the residual rotation of coupling beam exceeds φ_{re}, then as discussed by Mansour et al. (2011), the web connection of the replacement shear link might not be achieved by bolting and may require postdrilling holes or welding.

Conclusions

A series of quasi-static tests were conducted to examine the seismic behavior of replaceable steel coupling beams. Major findings from the study are summarized as follows:

(1) Three of the four replaceable coupling beams examined in this study exhibited excellent performance far exceeding the rotation demand of 0.02 rad that was computed for a prototype building.

(2) The replaceable coupling beam that adopted the end plate connection with shear key and high-strength bolts exhibited very stable hysteretic behavior and developed a large inelastic rotation of 0.06 rad. No slippage of bolts was observed, but local deformation of the end plates caused some connection rotation.

(3) The replaceable coupling beams that adopted the splice plate connection and bolted web connection developed an inelastic rotation of 0.08 and 0.06 rad, respectively. Bolt slippage in connections contributed significantly to coupling beam rotation and caused “pinching” in hysteresis loops.

(4) The replaceable coupling beam that adopted adhesive web connection failed early due to brittle failure of the adhesive.

(5) The I-shaped shear links with a length ratio of 0.7 had an inelastic rotation capacity of over 0.14 rad and an overstrength factor of 2.0, significantly exceeding the values specified for EBF links in AISC 341-10 (AISC 2010). The double channel link with a length ratio of 1.24 had an inelastic rotation capacity of 0.12 rad, and an overstrength factor of 1.5.

(6) An axial force in the coupling beam could arise because the axial deformation of shear links is restrained by adjacent wall piers. Tensile force accompanied large inelastic rotation, and subsequently, compressive force arose when the elongated coupling beam was unloaded to zero rotation. The maximum tensile and compressive forces reached approximately a quarter to half of the axial yield strength of shear link.

(7) Replacement of the link with end plate connection required the least effort and time, while the bolted web connection could accommodate the largest residual deformation that allows for easy replacement.

Acknowledgements

The work presented in this paper was sponsored by the International Science & Technology Cooperation Program of China (Grant No. 2014DFA70950), Tsinghua University Initiative Scientific Research Program (Grant No. 2012THZ02-1) and National Natural Science Foundation of China (Grants No. 51261120377 and No. 91315301). The writers wish to express their sincere gratitude to the sponsors.

Reference

AISC (American Institute of Steel Construction). (2010a). "Seismic provisions for structural steel buildings." *ANSI/AISC 341-10*, Chicago.

AISC (American Institute of Steel Construction). (2010b). "Specification for structural steel buildings." *ANSI/AISC 360-10*, Chicago.

ASCE (American Society of Civil Engineering). (2010). "Minimum design loads for buildings and other structures". *ANSI/ASCE 7-10*, Reston, VA.

Christopoulos, C., and Montgomery, M. S. (2013). "Viscoelastic coupling dampers (VCDs) for enhanced wind and seismic performance of high-rise buildings." *Earthquake Eng. Struct. D.*, 42(15): 2217-2233.

Chung, H. S., Moon, B. W., Lee, S. K., Park, J. H., and Min, K. W. (2009). "Seismic performance of friction dampers using flexure of RC shear wall system." *Struct. Des. Tall. Spec.*, 18(7): 807-822.

CMC (China Ministry of Construction). (2003). "Code for design of steel structures." *GB 50017-2003*, Beijing (in Chinese).

CMC (China Ministry of Construction). (2010). "Code for seismic design of buildings." *GB 50011-2010*, Beijing.

Fortney, P. J., Shahrooz, B. M., and Rassati, G. A. (2007). "Large-scale testing of a replaceable "fuse" steel coupling beam." *J. Struct. Eng.*, 133(12): 1801-1807.

Ji, X., Sun, Y., Qian, J., and Lu, X. (2015a). "Seismic behavior and modeling of steel reinforced concrete (SRC) walls." *Earthquake Eng. Struct. D.*, 44(6): 955-972.

Ji, X., Wang, Y., Ma, Q., and Qian, J. (2015b). "Experimental study on seismic behavior of replaceable steel coupling beams." *J. Build. Struct.*, 36(10): 1-10 (in Chinese).

Ji, X., Wang, Y., Ma, Q., and Okazaki, T. (2016). "Cyclic behavior of very short steel shear links." *J. Struct. Eng.*, 142(2): 04015114.

Kasai, K., and Popov, E. P. (1986). "A study of seismically resistant eccentrically braced frames." *Rep. No. UCB/EERC-86/01*, Earthquake Engineering Research Center, University of California, Berkeley.

Kulak, G. L., Fisher, J. W., and Struik, J. H. A. (1987). *Guide to design criteria for bolted and riveted joints*, 2nd Ed., Wiley, New York.

Kulak, G. L., and Green D. L. (1990). "Design of connectors in web-flange beam or girder splices." *Eng. J.*, 27(2), 41-48.

Kumagai, H., Shimazaki, K., and Hayashi, S. (2009). "Experimental study on coupling beams with steel dampers in mid-span." *J. Struct. Constr. Eng.*, 74(638): 755-763 (in Japanese).

Lu, X., Chen, Y., and Jiang, H. (2013). "Research progress in new replaceable coupling beams." *J. Earthquake Eng. Eng. Vib.*, 2013, 33(1): 8-15 (in Chinese).

Malley, J. O., and Popov, E. P. (1984). "Shear links in eccentrically braced frames." *J. Struct. Div.*, 110(9):2275-2295.

Mansour, N., Christopoulos, C., and Tremblay, R. (2011). "Experimental validation of replaceable shear links for eccentrically braced steel frames." *J. Struct. Eng.*, 137(10): 1141-1152.

McDaniel, C. C., Uang, C. M., and Seible, F. (2003). "Cyclic testing of built-up steel shear links for the new Bay Bridge." *J. Struct. Eng.*, 129(6), 801-809.

Murray, T. M., and Summer, E. A. (2003). "Extended end-plate moment connection, Seismic and wind applications." *Steel Design Guide Series 4 (2nd Ed.)*. American Institute of Steel

Construction, Chicago.

Okazaki, T., Arce, G., Ryu, H. C., and Engelhardt, M. D. (2005). "Experimental study of local buckling, overstrength, and fracture of links in eccentrically braced frames." *J. Struct. Eng.*, 131(10): 1526-1535.

Okazaki, T., and Engelhardt, M. D. (2007). "Cyclic loading behavior of EBF links constructed of ASTM A992 steel." *J. Constr. Steel. Res.*, 63(6):751–765.

OpenSees [Computer software]. Berkeley, CA, Pacific Earthquake Engineering Research Center (PEER).

Popov, E. P., and Engelhardt, M. D. (1988). "Seismic eccentrically braced frames." *J. Constr. Steel. Res.*, 10: 321–354.

Salmon, C. G., Johnson, J. E., and Malhas, F. A. (2009). "Steel Structures-Design and behavior" (5th Ed.), Pearson Prentice Hall, New Jersey.

Shahrooz, B. M., Remmetter, M. E., and Qin, F. (1993). "Seismic design and performance of composite coupled walls." *J. Struct. Eng.*, 119(11): 3291-3309.

Teshigawara, M., Kato, M., Sugaya, K. and Matsushima, Y. (1998). "Energy absorption mechanism and the fluctuation of shear force in the coupled shear walls." *Proc, Structural Engineering World Wide 1998,* Elsevier, San Francisco.

Table 1. Parameters of shear links

Spec. No.	Section	Web steel	Length ratio $e/(M_p/V_p)$	Flange width-to-thickness ratio $b_f/(2t_f)$	Web width-to-thickness ratio h_0/t_w	Stiffener thickness (mm)	Stiffener spacing (mm)
CB1	I 350×170×10×12	LY225	0.70	7.1	32.6	10	180
CB2	I 350×170×10×16	LY225	0.76	5.3	31.8	10	180
CB3	Double C 320×85×5×12	Q235	1.24	7.1	59.2	8	116
CB4	Double C 320×85×5×12	Q235	1.02	7.1	59.2	8	116

Table 2. Material properties for steel of shear links

Steel type	Plate	Thickness t (mm)	Yield strength f_y (MPa)	Ultimate strength f_u (MPa)	f_y/f_u	Elongation δ (%)
LY225	Web of CB1 and CB2	10	228	330	0.69	54.0
Q235	Web of CB3 and CB4	5	316	425	0.74	35.9
Q235	Stiffener of CB1 and CB2	10	273	432	0.63	44.4
Q345	Flange of CB1, CB3 and CB4	12	396	557	0.71	44.4
Q345	Flange of CB2	16	378	537	0.70	48.0

Table 3. Damage and failure process of specimens

Spec. No.	Rotation of coupling beam at damage occurrence (rad)						Failure mode
	Link-to-beam connection damage		Shear link damage				
	Adhesive failure	Bolt slippage	Web buckling	Stiffener-to-flange weld fracture	Web fracture	Flange-to end plate weld fracture	
CB1	—	—	0.04	0.04	0.04	0.05	Link flange-to end plate weld fracture
CB2	—	0.03	0.07	0.07	0.08	—	Link web fracture
CB3	—	0.03	0.05	—	0.06	—	Link web fracture
CB4	0.005	—	—	—	—	—	Adhesive failure

Table 4. Shear strength of specimens

Spec. No.	Plastic shear strength V_p (kN)	Maximum shear strength V_{max} (kN)	Overstrength Ω
CB1	446.0	926.4	2.08
CB2	435.0	837.5	1.93
CB3	561.2	880.4	1.57

Table 5. Deformation capacity of specimens

Spec. No.	Steel coupling beam	Shear link	
	Inelastic rotation capacity φ_p (rad)	Inelastic rotation capacity γ_p (rad)	Cumulative plastic rotation $\sum\gamma_p$ (rad)
CB1	0.06	0.18	4.37
CB2	0.08	>0.14	>4.74
CB3	0.06	0.12	1.85

Note：For Specimen CB2, the value of 0.14 rad link rotation corresponded to 0.07 rad coupling beam rotation. The LVDTs mounted at shear link were removed after 0.14 rad link rotation, as the deformation was out of their measurement range.

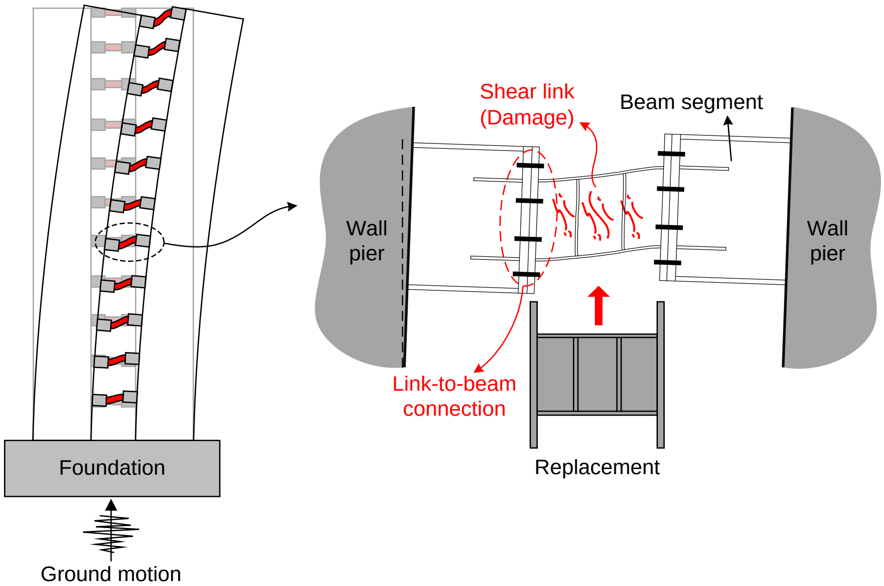

Fig. 1. Replaceable steel coupling beam

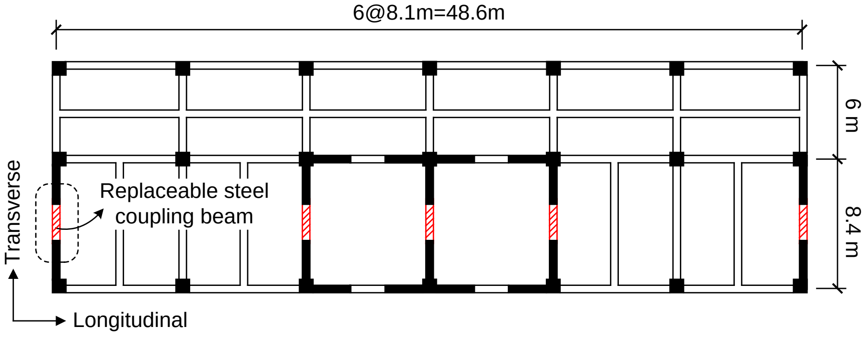

Fig. 2. Plan dimension of prototype structure

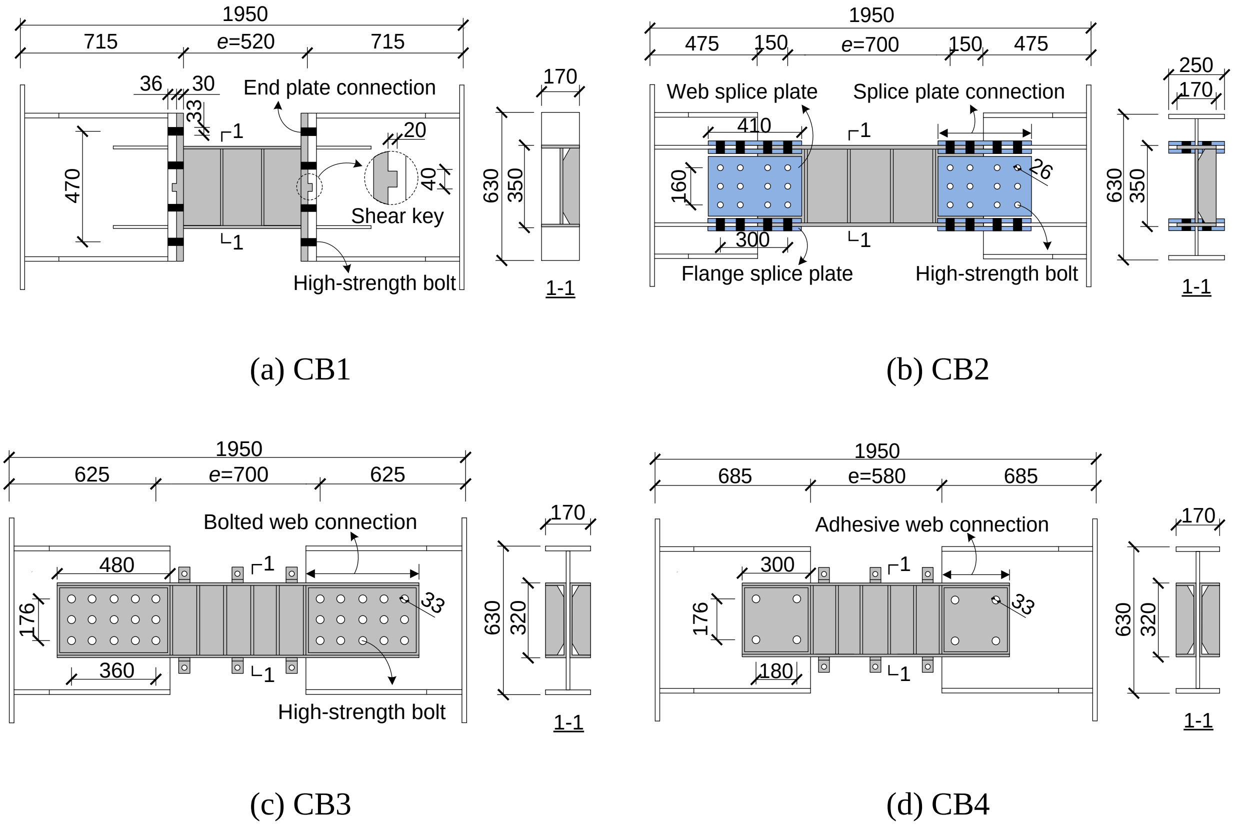

(a) CB1

(b) CB2

(c) CB3

(d) CB4

Fig. 3. Test specimens

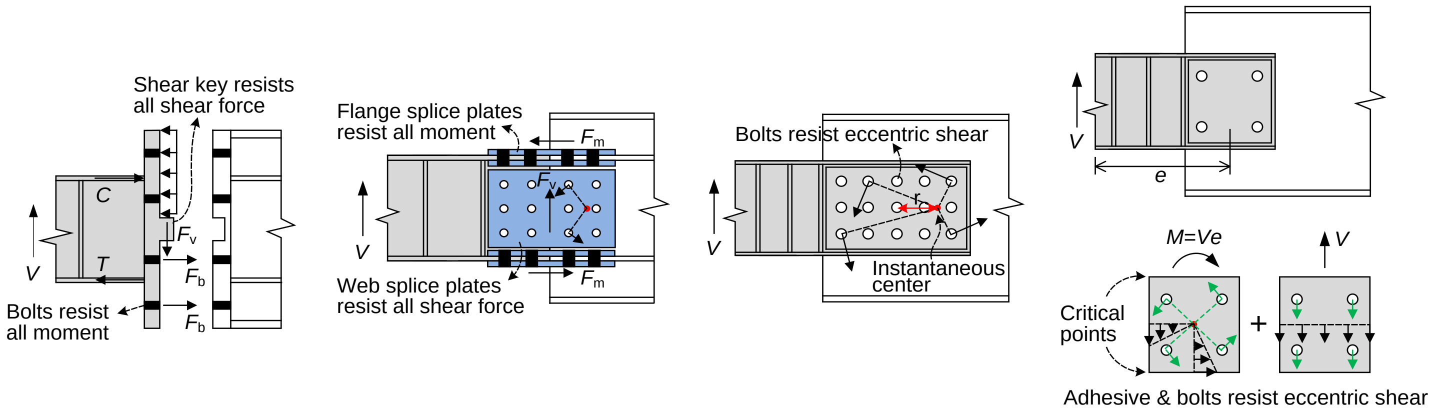

(a) CB1 (b) CB2 (c) CB3 (d) CB4

Fig. 4. Free-body diagram of link-to-beam connections

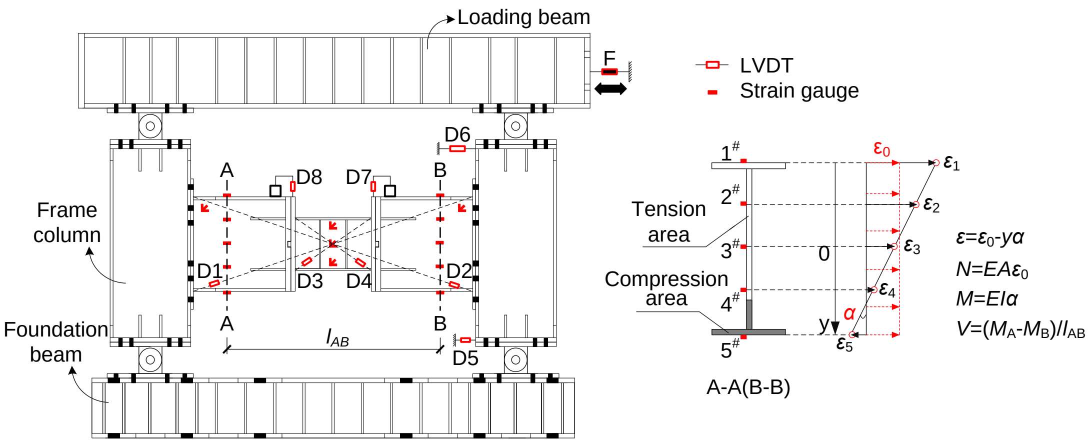

Fig. 5. Test setup and instrumentation

545

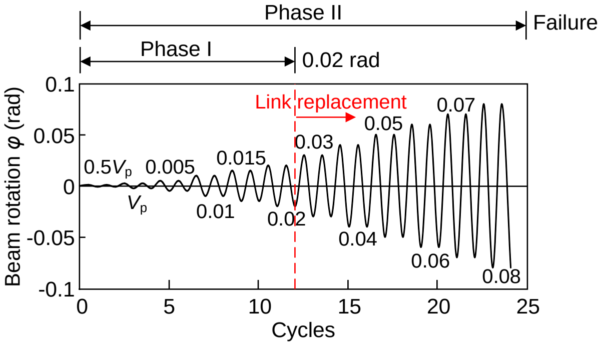

Fig. 6. Loading protocol

546

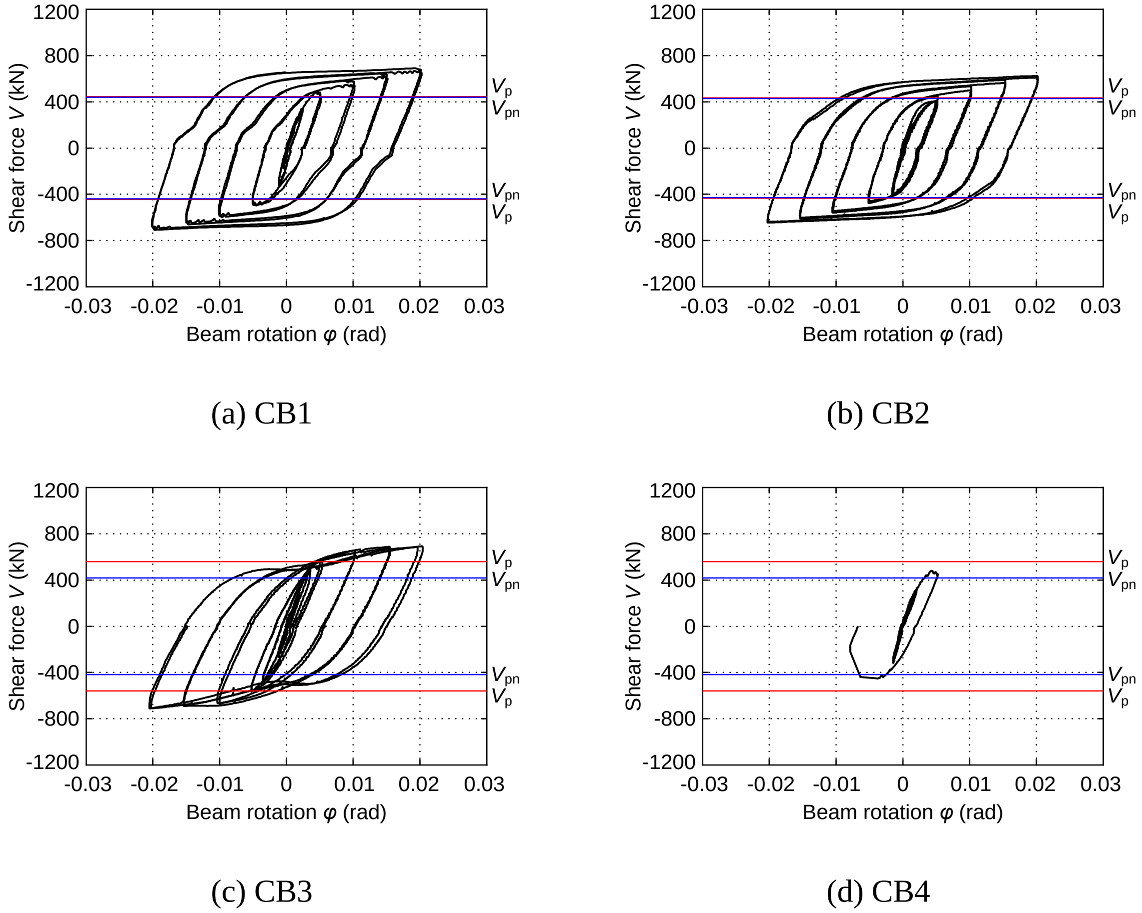

Fig. 7. Hysteretic responses of specimens in Phase I loading

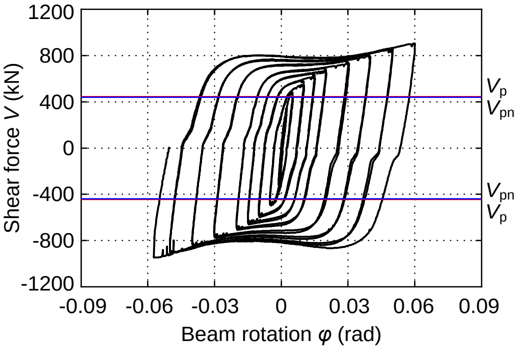

(a) CB1

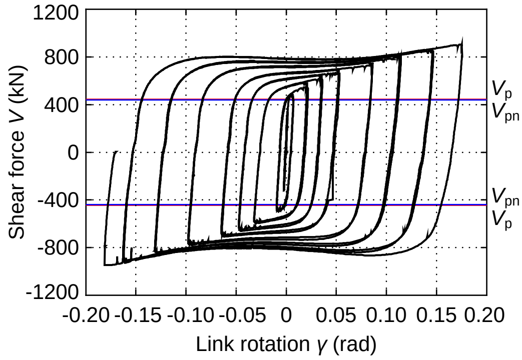

(b) Shear link of CB1

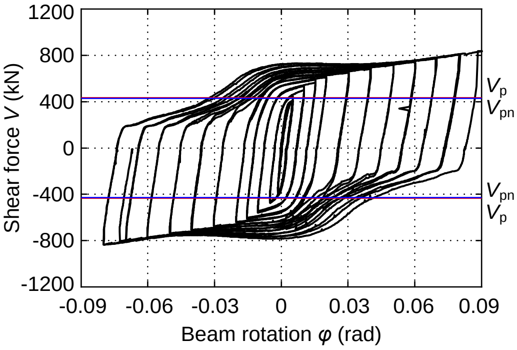

(c) CB2

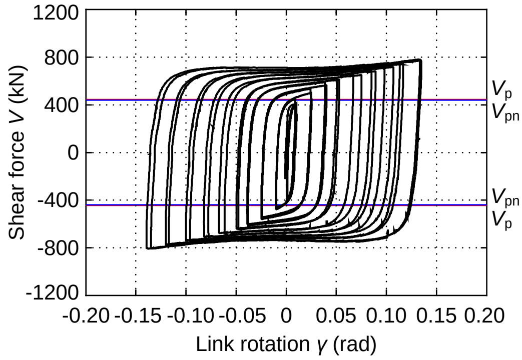

(d) Shear link of CB2

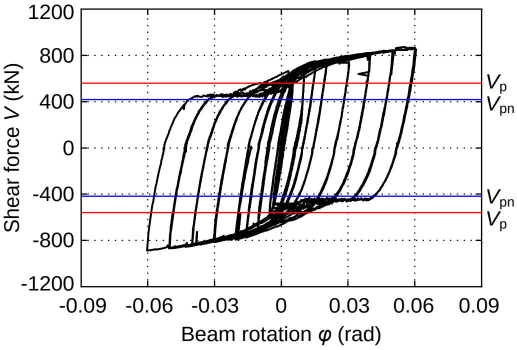

(e) CB3

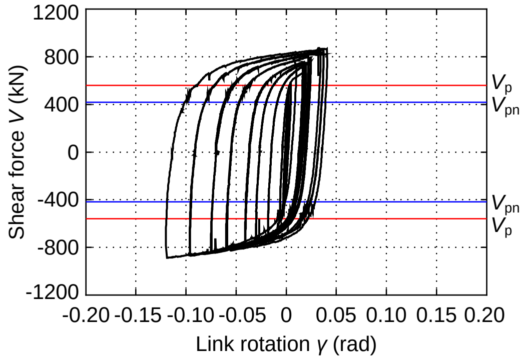

(f) Shear link of CB3

Fig. 8. Hysteretic responses of specimens and shear links in Phase II loading

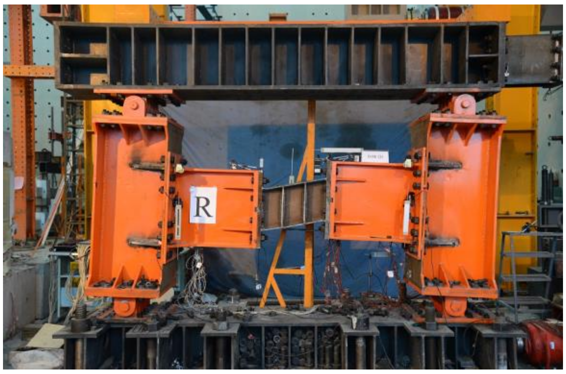

(a) CB1 at the end of the test

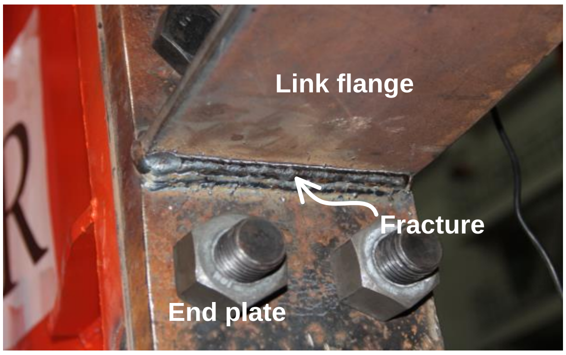

(b) Link flange-to-end plate weld fracture

(CB1)

(c) CB2 at the end of the test

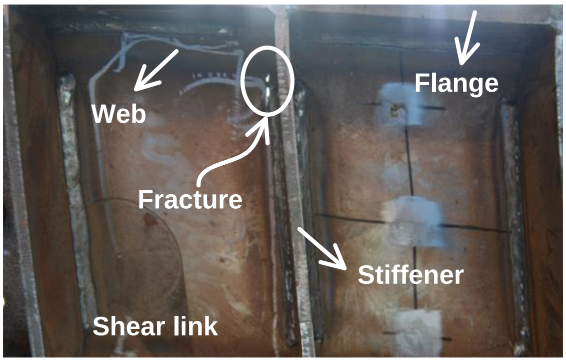

(d) Link web fracture (CB2)

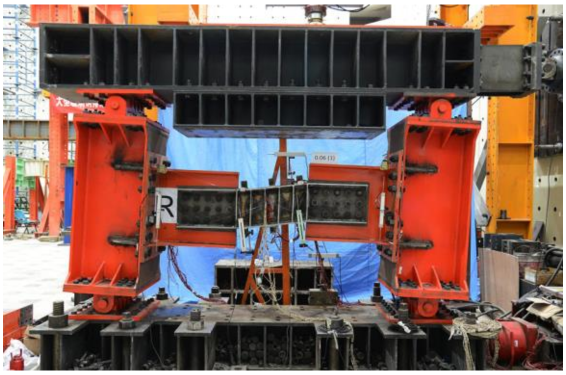

(e) CB3 at the end of the test

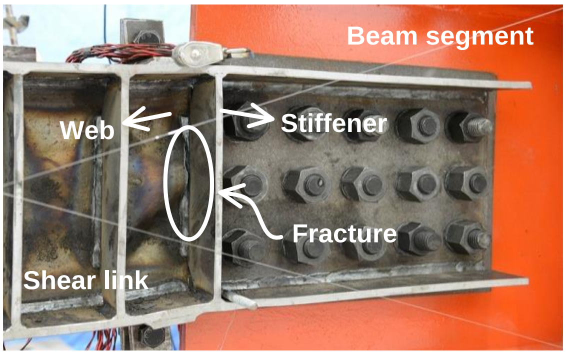

(f) Link web fracture (CB3)

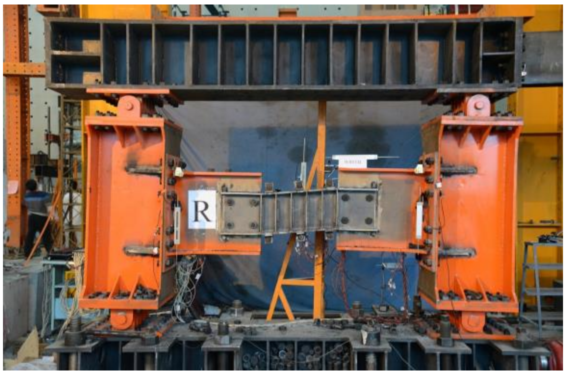

(g) CB4 at the end of the test

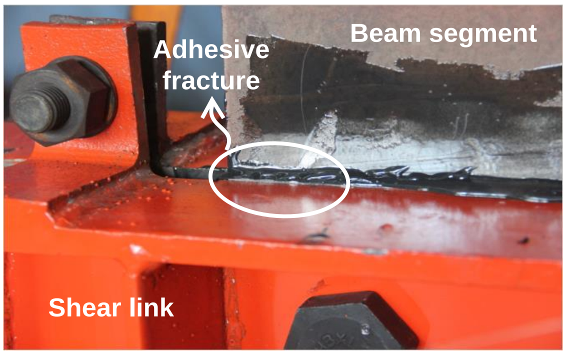

(h) Adhesive fracture (CB4)

Fig. 9. Photographs of specimens at failure

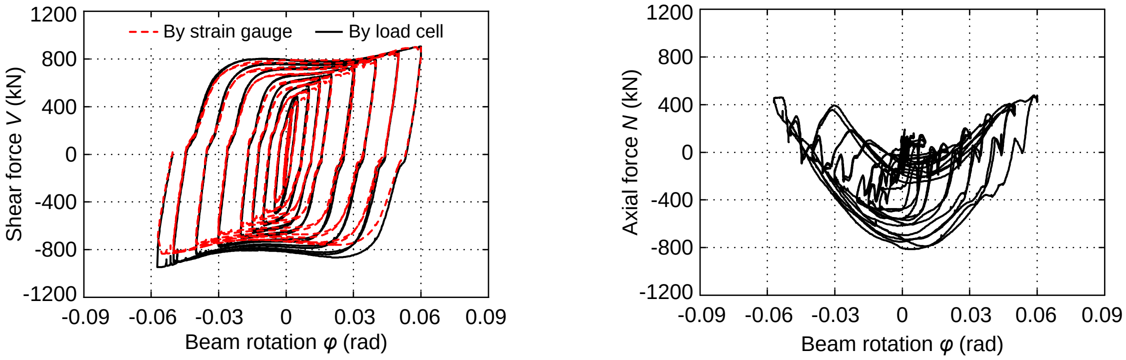

(a) Shear force (b) Axial force

Fig. 10. Inner forces of Specimen CB1

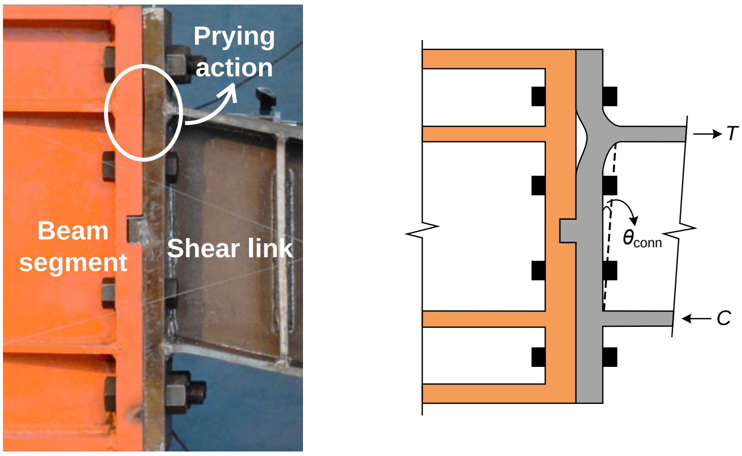

(a) Photograph of CB1 connection (b) Schematic drawing

Fig. 11. Local deformation in end plate connection

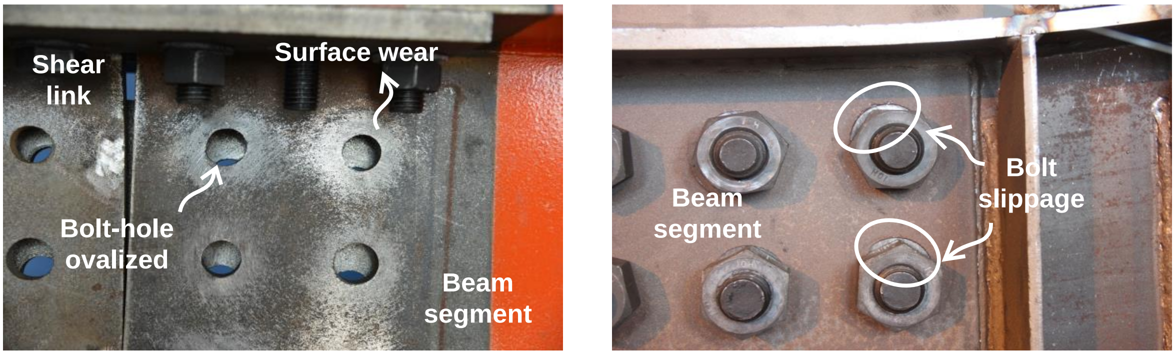

(a) CB2 (b) CB3

Fig. 12. Photographs of bolt slippage details

559

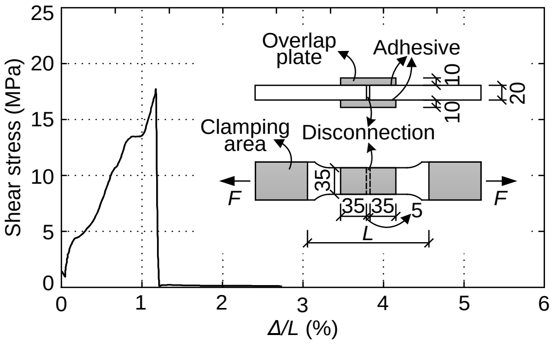

Fig. 13. Shear strength-deformation curve of epoxy adhesive

560

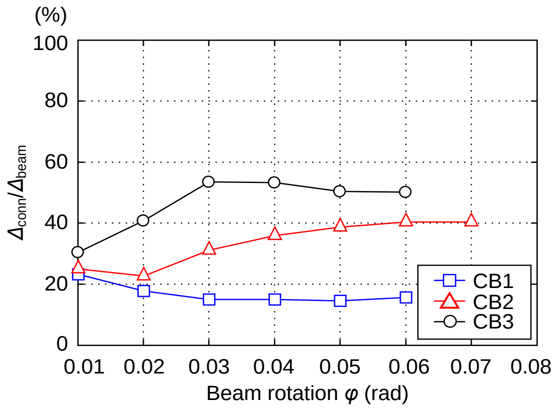

Fig. 14. Ratio of deformation induced by connection rotation

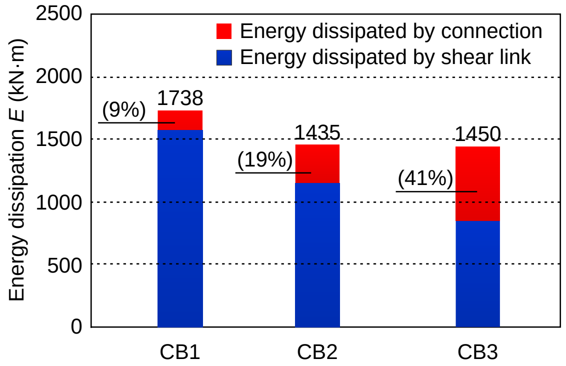

Fig. 15. Cumulative energy dissipation

Fig. 1. Replaceable steel coupling beam

Fig. 2. Plan dimension of prototype structure

Fig. 3. Test specimens: (a) CB1; (b) CB2; (c) CB3; (d) CB4

Fig. 4. Free-body diagram of link-to-beam connections: (a) CB1; (b) CB2; (c) CB3; (d) CB4

Fig. 5. Test setup and instrumentation

Fig. 6. Loading protocol

Fig. 7. Hysteretic responses of specimens in Phase I loading: (a) CB1; (b) CB2; (c) CB3; (d) CB4

Fig. 8. Hysteretic responses of specimens and shear links in Phase II loading: (a) CB1; (b) Shear link of CB1; (c) CB2; (d) Shear link of CB2; (e) CB3; (f) Shear link of CB3

Fig. 9. Photographs of specimens at failure: (a) CB1 at the end of the test; (b) Link flange-to-end plate weld fracture (CB1); (c) CB2 at the end of the test; (d) Link web fracture (CB2); (e) CB3 at the end of the test; (f) Link web fracture (CB3); (g) CB4 at the end of the test; (h) Adhesive fracture (CB4)

Fig. 10. Inner forces of Specimen CB1: (a) Shear force; (b) Axial force

Fig. 11. Local deformation in end plate connection: (a) Photograph of CB1 connection; (b) Schematic drawing

Fig. 12. Photographs of bolt slippage details: (a) CB2; (b) CB3

Fig. 13. Shear strength-deformation curve of epoxy adhesive

Fig. 14. Ratio of deformation induced by connection rotation

Fig. 15. Cumulative energy dissipation